Towards solar iron metallurgy: Complete hydrogen reduction of iron ore pellets under a concentrated light flux

Bastien Sanglard, Bertrand Huneau, Julian Carrey, Sébastien Lachaize

Towards solar iron metallurgy: complete hydrogen reduction of iron ore pellets under a concentrated light flux

B. Sanglard[1], B. Huneau[2], J. Carrey[1] and S. Lachaize[1]

[1] Laboratoire de Physique et Chimie des Nano-Objets (LPCNO), Université de Toulouse, INSA, CNRS, UMR 5215, UPS, 135 Avenue Rangueil, F-31077 Toulouse, France

[2] Institut de recherche en Génie Civil et Mécanique (GeM), Nantes Université, École Centrale Nantes, CNRS, UMR 6183, F-44000 Nantes, France

Abstract: Current ironmaking process leads to large CO_2 emissions due to the use of fossil fuels as both heating agent and reducer. An alternative ironmaking process based on the reduction of iron ore by hydrogen under a concentrated light flux, simulating a direct solar heating reactor, is studied here. Experiments were performed in batch mode on the iron ore pellets used in industry, which consist in spherical agglomerates of iron oxide with a diameter of ca. 2 cm. Quantitative analysis of the reduction yield and kinetics were deduced from the Rietveld refinements of X-ray diffraction patterns as well as optical and scanning electron microscopy. It is shown that hydrogen pressure has a significant influence on the time evolution of the reaction, probably by its influence on re-oxydation. Observations and analysis of cut pellets show that reduction starts from the illuminated surface towards the shadowed side, due to a large temperature gradient inside the sample. This conducted us to perform experiments in which pellets were rotated, which significantly reduce reduction time. On single pellets, a reduction yield of 96% was reached in 12 min by turning them three times during exposure. Samples under the form of gravels and flat disks were also tested. The former did not lead to significant improvement, but a 96% reduction yield was measured on 2-mm-thick disks after only 2 minutes of exposure. An analysis of the energy efficiency of the process is provided. These results show that hydrogen-based solar metallurgy could meet industrial requirements in terms of reduction yields and might be envisaged as a low-carbon ironmaking process.

Keywords: Hydrogen, Concentrated solar power, Metallurgy, Iron, Mitigation, CO_2 emissions

I. Introduction:

Iron and steelmaking industry is responsible for large greenhouse gas emissions, representing close to 6.7% of global anthropogenic CO_2 emissions [1]. Additionally, the ironmaking process has a crucial importance in our society since steel is one of the most used materials worldwide. To respect the +1.5 °C limit of Paris agreement, the emissions from the steelmaking industry should drop from 1.85 t CO_2/t steel to 0.6-0.3 t CO_2/t steel by 2050 in a perspective of a 38% production growth [2]. The most used route to produce steel is the integrated route, which consists in transforming iron ore (mainly composed of hematite and small amounts of magnetite and other mineral oxides) into liquid pig iron (iron-carbon alloy containing up to 5% of carbon) using coal. Some carbon is then removed from pig iron in an oxygen furnace, leading to steel. This route produces alone 71% of the total crude steel used worldwide and emits approximately 2.2 tCO_2/t steel [3]. Another well-known and largely used way to produce iron is direct reduction, which consists in a solid-state reduction of iron ore by different reducing gas (CO and/or H_2) at a temperature around 950 °C. The reducing gases mainly originate from coal and natural gas, but can also be produced by biomass pyrolysis [4]. When the reducing agent is carbon monoxide, the reaction contributes to greenhouse gas emissions as shown in Equation (1) [4]:

$$3\,Fe_2O_3 + 3\,CO \rightarrow 2\,Fe + 3\,CO_2 \qquad \Delta H^o_{298} = -209\,k_J\,/kg\ of\ Fe \qquad (1)$$

The direct reduced iron (DRI) is then melted with carbon in an electric arc furnace to form steel. Globally, direct reduction route leads to lower emissions than the integrated one: 1.95 tCO_2 / t steel and 1.4 tCO_2/ t steel for the coal-based and the gas-based route, respectively [3].

Industries and laboratories have investigated several routes to reduce the greenhouse gas emissions of the ironmaking processes. For the integrated route, reduction of the amount of coke used, optimization of the reducer/ore ratio, recycling of the exhaust gas, improvement of the upstream process (coking, smelting) are pathways to diminish the ecological weight of the process [5]. Additionally, Suopajärvi *et al.* have shown that coal consumption and consequently CO_2 emissions could be significantly reduced when partly substituting coal with charcoal, torrefied wood or bio-synthetic natural gas [6]. Unfortunately, they also noted that

the production cost of such reducers would be a drawback for this technology. Moreover, the availability of the biomass resource would also be a serious issue.

For the direct reduction route, the most studied alternative is based on the use of hydrogen as reducing agent, which forms water as by-product. The reaction goes through different intermediates according to temperature as shown by the Chaudron phase diagram (see Supplementary Information (S.I.) Figure A-1) [4]. For temperatures below 570 °C, magnetite (Fe_3O_4) is formed before reduced iron [7]:

$$3\,Fe_2O_3 + H_2 \rightarrow 2Fe_3O_4 + H_2O \quad (2)$$

$$Fe_3O_4 + 4H_2 \rightarrow 3Fe + 4H_2O \quad (3)$$

For temperatures higher than 570 °C, both magnetite and wustite (FeO) are formed [7]:

$$3\,Fe_2O_3 + H_2 \rightarrow 2Fe_3O_4 + H_2O \quad (4)$$

$$Fe_3O_4 + H_2 \rightarrow 3FeO + H_2O \quad (5)$$

$$FeO + H_2 \rightarrow Fe + H_2O \quad (6)$$

The reduction of wustite [Equation (6)] is the limiting step of the overall kinetics of the reaction.

The use of hydrogen as a low-carbon reducer has already been studied, as reviewed by Heidari *et al.* [8]. Wagner *et al.* showed that the reduction rate rises with temperature [9]. Choi and Sohn studied the high temperature (900-1500 °C) reduction of iron ore small particles (< 100 μm) and showed that at 1200 °C the particles were reduced over 90% in 1.6 s with around 1000% of H_2 excess. At 1300 °C, around 90% of the reduction was achieved in 2.4 s with 240% of H_2 excess [10]. Hydrogen is also used as reducing agent by companies working with the DRI process (*e.g.* Midrex [11]) and is planned to be more and more used (Hybrit project [12]). Ammonia has also been studied as a carbon-free reducer [16, 17, 18]. For instance, Hosokai *et al.* showed that 0.27 g of pure hematite could be reduced completely at 600°C and 700°C after respectively 2h and 1h.

However, the hydrogen route is intensive in electricity when green hydrogen – i.e. produced by electrolysis using low-carbon electricity – is used. Indeed, the energy consumption to produce iron from green hydrogen represents 3.5 MWh_e/t steel, with approximately 70% due to the production of green hydrogen itself [14]. As comparison, the integrated route uses 356 kWh_e/t steel and the DRI route 1.2-1.3 MWh_e/t steel [3]. Among the later, the melting of the

DRI in the EAF furnace is the main item of consumption : it has been estimated to 918 kWh/t of steel by Fan *et al.* [3] and to 753 kWh/t by Vogl *et al.* [14]. Provided that 1.9 Gt of steel were produced in 2023 [15], maintaining the current level of iron production with green hydrogen would require 6 622 TWh of low-carbon electricity. This value corresponds to 22% of the electricity produced worldwide the same year (29 471 TWh in 2023) [16]. Providing such an amount of low-carbon electricity in a few decades is a huge challenge, to say the least.

As already mentioned above, another way to reduce emissions in the integrated or DRI route would be to change the classically used coke to biochar or biogas. However, biomass resources – as low-carbon electricity – are also limited and should be shared with other industrial sectors. So decarbonating iron production at our current level of production in a few decades seems difficult; with a view to a sustainable future, it might even not be desirable to keep such a high level of production in reasons of the global upstream and downstream social and environmental impacts of iron (mining, artificialisation, infrastructures, …). Thus, an approach based on a more efficient steel use, on reuse and on low contamination recycling would lead to a decreased level of production, complementary of any low-carbon process. Sufficiency and lifestyle changes are also additional ways to induce a significant production decrease [17].

To efficiently reduce the CO_2 emissions of the DRI process, the contributions originating of both heat production and chemical reaction should be tackled. In this work, it will be studied the use of concentrated light flux to provide heat and hydrogen as reducer.

In this perspective, the use of solar concentrated power as a heat source has been studied before. For instance, in 1991, Steinfeld and Fletcher studied direct carbothermic reduction (reduction of hematite with solid carbon) under concentrated solar flux and were able to reach 78% of reduction yield at 2000 K [18]. In 1993, Steinfeld and Kuhn studied the reduction of magnetite (Fe_3O_4) under concentrated solar flux and methane atmosphere [19]. They were able to reach 68% of reduced iron from a dry mixture of magnetite and silica after heating it during 15 minutes at 1273 K in a solar oven. Fernández-González *et al.* studied the smelting reduction of hematite (Fe_2O_3) with carbon under solar flux and the one of sintered ore with coke breeze [20]. They were able to reach a maximum of 5.6% of reduced iron in the hematite sample at 1353 °C and 29.7% in the sintered oxide one, reaching a temperature high enough to melt the upper layer of the sample.

So far, only two studies of the combined use of hydrogen and solar energy for direct reduction has been recently published : Li *et al.* [21] and Abanades *et al.* [22]. First, Li *et al.* studied the reduction under hydrogen of hematite fine particles in an indirect solar heating reactor equipped with a vibrant fluidized bed and were able to reach 98% of reduction in 50 min. - Secondly, Abanades *et al.* studied the reduction of iron ore power (from 0.25 to 2 mm in diameter) in backed bed under solar irradiation. They showed a complete reduction after 15 min at 1000 °C and showed that the quantity of powder in the backed bed had an influence on the reduction rate.

The experiments described hereafter differs from both studies. First, they were conducted on the exact same pellets as the one used in industrial processes whereas iron ore power or hematite powder was used in the previous studies. Secondly, here, the reduction was realized by exposing directly the sample to concentrated light flux (direct reactor) where Li *et al.* and Abanades *et al.* used an indirect reactor. Moreover, in this work, several experimental parameters of the reduction were varied in order to understand the reaction mechanisms and to reach high reduction yield in a short time.

This article is organised as follows. First, test bench, samples and methods are described. Second, the influence of various parameters (pressure, time, power) is shown. Third, results to optimize the reduction time and yield are presented, as well as an energy analysis. Finally, the results are discussed before providing a general conclusion.

II. Materials and methods:

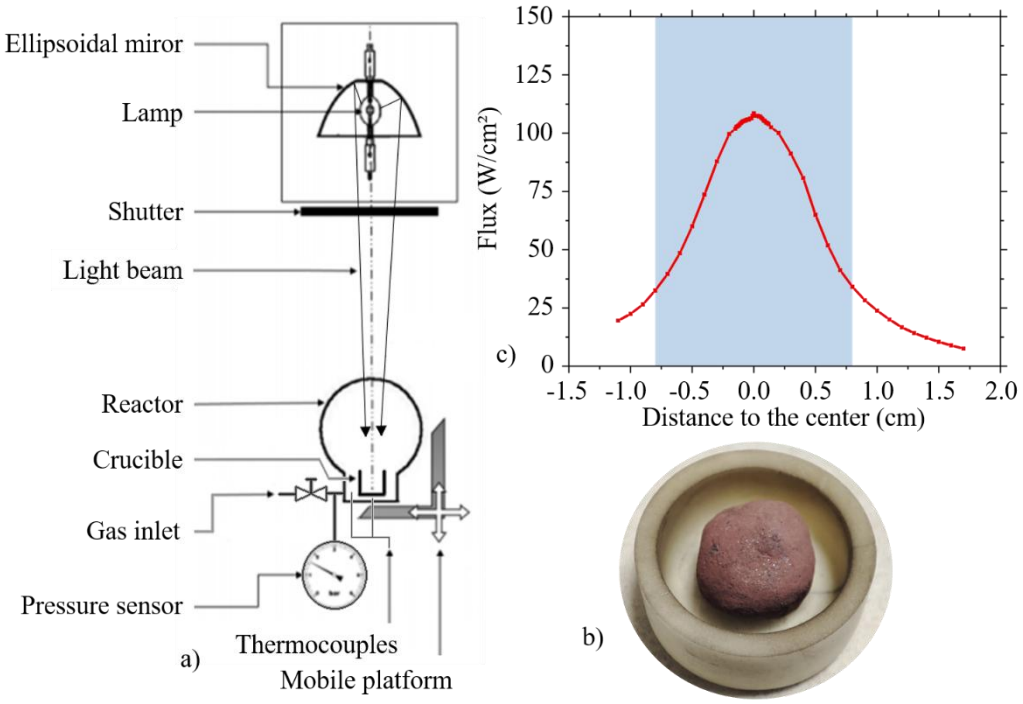

Figure 1: (a) Schematic of the solar simulator bench used for the experiments. (b) Detail picture of the crucible holding a typical iron ore pellet (crucible A). (c) Light flux measurement over the crucible radius.

Experiments were realised using the experimental set-up shown in Figure 1-a. The bench is composed of a Xe lamp (electric power of 1600 W_e, 9 mm long arc) placed at the focal point of an ellipsoidal mirror (XE1600, Sciencetech). The total light power at the output of the reflector was calculated by performing a series of flux measurements (flux meter TG1000-0, Vatell) over the complete radius of the light spot (see Figure 1-c). The total power is then obtained after an integration of the curve. An alumina crucible (diameter: 16 mm, Sceram ceramics) is placed inside a 0.6 L borosilicate glass reactor resistant to 10 bars of gas pressure. This reactor is placed on a mobile XY platform (Thorlabs – two XR25C mounted at 90°), the displacement over the Z axis being realised with a homemade rack and pinion. The crucible was placed a few centimetres below the focal point to be more homogeneously illuminated. At this position, a power of about 140 W was measured, corresponding to a mean flux of 70 W/cm^2 (see Figure 1-c). The temperature is measured with two K-type thermocouples: one placed right under the crucible and the other one in the atmosphere but not directly under the light flux. The pressure inside the reactor is measured with a sensor (type 520, Huba control). Both temperature and pressure are acquired in real-time using a homemade Labview program. Before each experiment, the reactor is successively vacuumed and refilled three times with the reducing gas before setting it at the required pressure; each

experiment was thus performed under a static atmosphere condition. The hydrogen is produced by water electrolysis using a H_2 generator (F-DGSi, model WM-H2, O_2 < 0.01 ppm and moisture < 1 ppm). After the experiment, samples are left to cool before being placed in the ambient atmosphere and analysed.

The samples used for the experiments were industrial grade iron ore pellets used in the DRI process, courtesy of the ironmaking company ArcelorMittal (Metz, France). They are mainly composed of iron oxide (> 97%) with a small amount of standard impurities (Si, Al, Ca, MgO). The composition provided by the furnisher can be found in S.I. Table B-1.

First, reduction experiments under different conditions were realised by placing the sample in a 2.0 cm² area crucible (crucible A, see Figure 1-b) under several pressures and exposure times. The pressure studied were 1, 2 and 4 bars to determine which minimal pressure was acceptable to ensure the sample reduction and to prevent its re-oxidation by the water vapor produced during reduction [19], [23]. The maximum of 4 bars allows to be far from the safety limit of our glass reactor even at the end of the experiments since pressure increases all along the reduction process. Additionally, the longest exposure time of 28 minutes was chosen after preliminary experiments showing a significant reduction yield of iron ore powder after this duration. For these series of experiments, only the quantitative advancement of the reduction was studied and not the reduction yield itself. To this end, the samples were dried before the experiments at least 1 week into a proofer at 110 °C and weighted before and after reduction. This allowed to access the oxygen loss value, which is a good indicator of the quantitative advancement of the reduction.

Other experiments were realized to observe specifically the way the reduction proceeds inside the samples. Firstly, the exposure time was varied from 0.5 min to 16 min under 60 W/cm². Secondly, 4 min reductions under different mean light density flux values were performed (46 W/cm², 54 W/cm², 60 W/cm², 65 W/cm² and 75 W/cm²). For each varied parameter, measurements were realised on two series of pellets. In each series, their masses differed by less than 5% (see Table 1). The pellets were cut in half vertically and observed using optical microscopy. The surface of the iron phase compared to the oxide one was measured using ImageJ software by contouring each surface. EDX mapping was also realised using a SAMx detector on a JEOL 6060-LA SEM.

Table 1 : Conditions of the performed reduction experiments.

Varied	Variation	Samples	Masses (g)	Mean	H_2	Note

parameter				diameter (cm)	pressure (bar)	
Exposure time	0.5 to 16 min	Serie 1	2.11 to 2.19	1.05	2	60 W/cm²
		Serie 2	2.29 to 2.38	1.14	2	
Light power density	46 to 75 W/cm²	Serie 3	2.18 to 2.25	1.13	2	4 min reductions
		Serie 4	2.33 to 2.38	1.13	2	

Finally, the reduction yield of the process was assessed and different ways were tested to reach high enough values with respect to industrial requirement (approx. 93-94% for the DRI process [24], [25]). To this end, the initial shape of the raw materials was changed into gravel or disks, by either grinding the pellet or by cutting it using a precision circular saw with diamond blade (Buehler IsoMet low speed saw; Buehler – n°114254). Experiments on disks were conducted using a specifically designed crucible (crucible B, see S.I. Figure E-3): it favours gas circulation by avoiding a direct contact between the bottom surface of the disk and the crucible; it also avoids shading the disk by the crucible walls.

To measure the reduction yield, samples were transformed in powder using mortar and pestle, and then analysed using an X-ray diffractometer (PANalytical Empyrean 45 mA 35 kV, Co). For experiments on pellets, the quantity of analysed powder represented between 1/4 and 1/3 of the pellet. For experiments on gravels, all the gravels present in the crucible were transformed into a powder which was analysed. Afterwards, Highscore software was used to identify the phases within the sample; MAUD software was then used to realize Rietveld refinements on the diffractograms to access the mass percentage of each phase. When the refinements were used, the contribution of the residual peaks was less than 1%. Finally, the experimental reduction yield was calculated by dividing the mass of metallic iron after reduction by the mass of iron-containing phases in the sample before reduction, as shown by Equation (7).

$$Reduction\ yield = \frac{\%_{Fe(0)}}{\%_{Fe_2O_3} + \%_{Fe_3O_4} + \%_{FeO} + \%_{Fe(0)}} \quad \# \ (7)$$

III. Results and discussion

III.1. Influence of pressure, exposure time and lamp power on reduction performances

Figure 2 presents the results of iron ore reduction under a solar simulated flux as a function of exposure time for different hydrogen pressures. The oxygen mass loss analysis was realised following the previously presented protocol. The interest of this analysis is to allow for a quick observation of the effect of experimental parameters on the reduction rate. At first sight, it can be observed in Figure 2 that the oxygen loss rises steeply during the first 4 min without significant influence of pressure. Afterwards and until 8 min the steepness of the curves lowers slightly but still without major influence of pressure. After 8 min, the curves split: the 4-bar curve continues to rise with a decrease in the steepness; the 2-bar curve plateaus; the 1 bar curve decreases. The splitting of the curves during the reaction is attributed to hydrogen consumption [26]; theoretically, to completely reduce one equivalent of Fe^{3+}, 1.5 equivalents of H_2 are necessary. At the beginning of the reaction, the H_2:Fe ratios are 1.55:1, 2.35:1 and 3.89:1 at 1, 2 and 4 bars respectively (the ratios were calculated using the iron oxide masses, the reactor volume and the stoichiometry of the reaction). Thus, at 1 bar pressure, there is only a small excess of hydrogen compared to the theorical value. So, as the reduction progresses and because the experiments are realised in batch, the competition between the water vapor formed and the remaining hydrogen lowers the activity of the latter, as previously discussed in the literature [27]. The decrease after 8 min of the 1 bar curve is interpreted as a re-oxidation of the sample due to the presence of a large excess of water. This behaviour has previously been reported for magnetite at temperatures between 100 and 500 °C [18, 21].

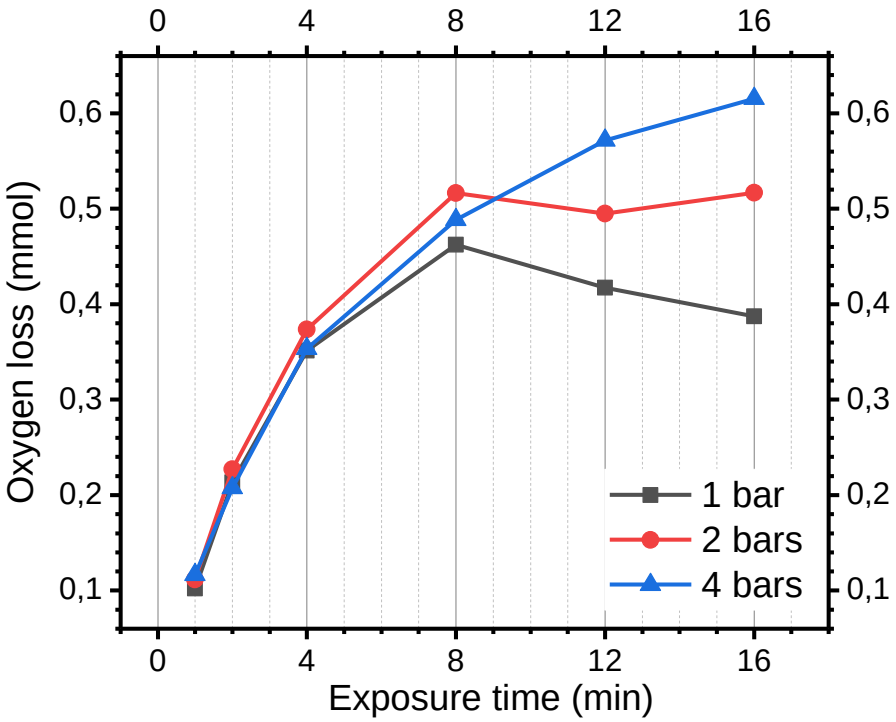

Figure 2: Oxygen loss as a function of the exposure time for various pressures of hydrogen (black: 1 bar; red: 2 bars; blue: 4 bars) after reduction of iron ore pellets under 60 W/cm². Each point of the curves represents a complete experiment.

Since the light flux is concentrated onto the top of the sample, the conditions are drastically different from a classic furnace. Therefore, it was decided to cut the reduced pellets in half (as shown in Figure 3-a) to observe the progression of the reduction front. Figure 3-b and c show the inside of two pellets exposed to the light flux during 2 and 7 min, respectively, the red line representing the reduction front. In the pictures, two zones with very different colours are observed. SEM observations coupled with EDX mapping show that the upper part (above the red line) of the sample is iron whereas the lower one (under the red line) is iron oxide. Quantitative analyses show that the transitions between the two materials occurs within ca. 0.5 mm (see S.I. Figures C-1). In a standard oven, the reduction of pellets is usually described by the shrinking core model: the reduction starts from the external surface of the pellets and goes towards the core of the pellets, thus creating an iron shell [28]. Here, the behaviour is different: because of light irradiation, the reduction starts from the top of the pellet and grows downwards, hence preserving the iron oxide in the shadowed side of the pellet. The reduction being temperature dependent, this reveals the presence of a temperature gradient within the pellet.

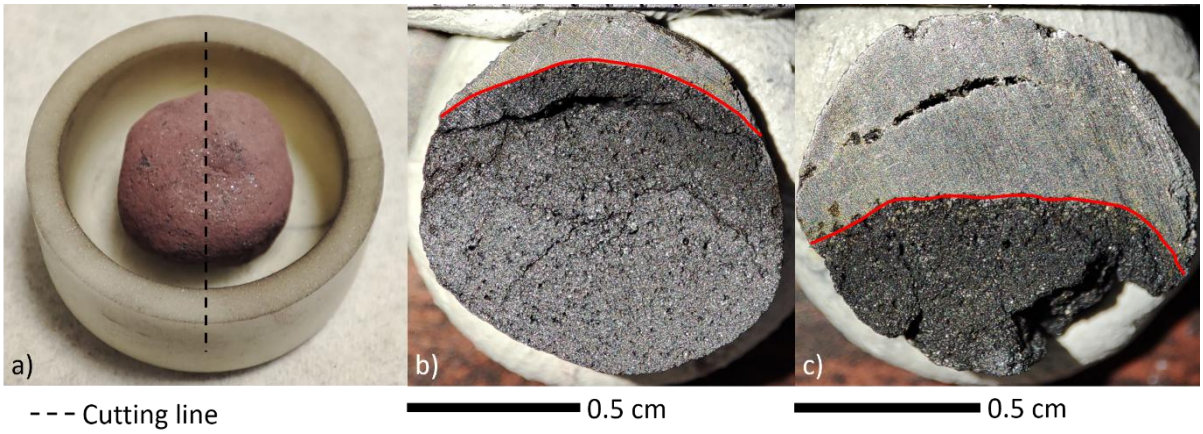

Figure 3: (a) Picture of a pellet in the crucible. The dotted line represents the profile on which the pellets were cut in half. Picture of a pellet after hydrogen reduction during (b) 2 min and (c) 7 min under 2 bars of hydrogen and 60 W/cm². The pellet was cut in two after the experiments to perform this observation. The red line represents the reduction front with the reduced iron above and the iron oxides below. Samples were illuminated from the top.

To quantify this progression, the surface of reduced iron for an exposure time varying from 0.5 min to 16 min as well as the total surface of the pellets were measured (see Figure 4). The surfaces were determined using the software ImageJ on images such as the ones shown in Figure 3-b and Figure 3-c. The corresponding pictures are available in S.I. Figures C-2 and C-3. Results show that the reaction rate follows an exponential decay tendency, plateauing or strongly slowing down after 10 minutes, before the reduction is complete. These pictures can also be used to estimate the reduced thickness per unit of time: it evolves from 2 mm/min at the very beginning to 0.3 mm/min before the plateau (between 7 and 10 min of reaction). Such a behaviour has previously been observed in the hydrogen reduction of pellets in an oven, and was interpreted as due to the slower diffusion rate of hydrogen in the reduced iron as opposed to the one in the porous oxide [29]. However, here, since the bottom of the pellet is clearly not reduced, hydrogen keeps it capability to feed the reaction toward the reduction front at the same rate. This result is therefore interpreted as resulting from a temperature gradient appearing inside the pellet and will be discussed more thoroughly in section III.3.

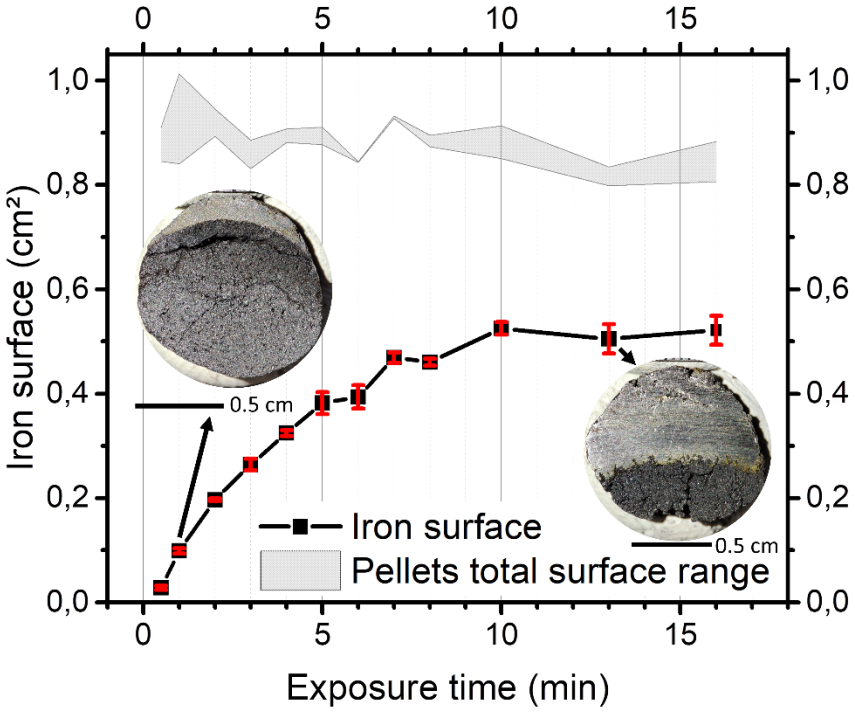

Figure 4: Iron surface evolution as a function of exposure time after the reduction of pellets under 2 bars of hydrogen and 60 W/cm² (square dots). The black line corresponds to the iron surface averaged over the two series, and the error bar to the standard deviation. The total surface of each of the two pellets used to measure one point is indicated as two grey-filled curves. Pictures of cut samples exposed for 2 min and 13 min are shown as insets.

Figure 5 shows the evolution of the iron surface as a function of the light flux density for 4 min of reduction under 2 bars as well as the total surface of the pellets. The later were cut as shown in Figure 3-a and corresponding pictures are shown in S.I. Figures D-1 and D-2. The surfaces were here again determined using the software ImageJ. As expected, the reduced surface increases with lamp power, evidencing the influence of temperature on reduction rate.

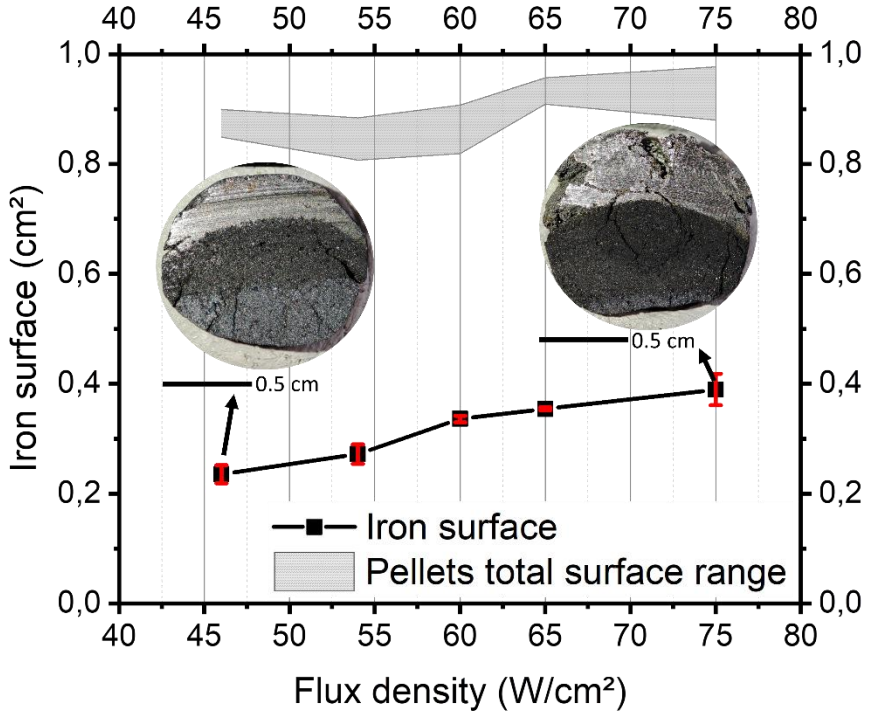

Figure 5: Iron surface after 4 min reduction under simulated solar flux and 2 bars of hydrogen for several light flux density: 46 W/cm², 54 W/cm², 60 W/cm², 65 W/cm² and 75 W/cm². The total surface of the pellets is indicated as two grey-filled curves. The black line corresponds to the iron surface averaged over the two series and the error bar to the standard deviation. Pictures of cut pellets for 46 W/cm² and 75 W/cm² are shown as insets.

III.2. Optimization of reduction yield and kinetics

The reduction rates observed in these experiments were of the same order of magnitude as the one found in the literature on hydrogen reduction [30], [31]. Nonetheless, in order to try to reduce exposure times, experiments consisting in turning over the pellets one or three times by 180° or 90°, respectively, were conducted. Similar experiments were also conducted on gravel. In the latter case, they were only shaken until a majority of them were turned. For experiments on both pellets and gravel, crucible A was used and the samples were allowed to cool down before being manually turned over radially or shaken.

Finally, optimization was attempted on three types of samples in order to study the impact of sample shape on the reduction yield and kinetics: i) pellets, ii) a single-layer of gravel of ca. 2.0 mm and iii) 2.0 (± 0.11) mm thick disks with different mean radius (7.7 mm, 5.9 mm and 4.5 mm). Since their thicknesses are similar, the disks are listed as function of their radius. Pictures of the gravel and the disks are available in S.I. Figures E-1 and Table E-1 respectively. Table 2 summarizes the structural properties of the various samples (pellets, gravel and disks), the experimental conditions, as well as the main results.

Table 2: Structural properties, experimental conditions and main results in the series of experiments aiming at maximizing the reduction yield (XRD quantification) under hydrogen atmosphere. The lamp flux density was 60 W/cm². A reactor with a constant volume of 0.6 L was used. For the temperature, the one of the disks are not informative because of the specific configuration of the experiments (cf S.I. Figure E-3).

Sample	*Sample type*	*Initial mass (g)*	*Pressure (bar)*	*Total exposure time (min)*	*Reduction yield (%)*	*Wustite percentage (%)*	*Temperature under the crucible (°C)*	*Note*
S1	*Gravel*	*0.37*	*2*	*28*	*88.4*	*11.6*	*412*	
S2	*Gravel*	*0.31*	*2*	*28*	*94.7*	*5.3*	*389*	*Turned over once by approx. 180°*
S3	*Pellet*	*1.70*	*3.5*	*28*	*83.8*	*14.5*	*371*	
S4	*Pellet*	*1.71*	*3.5*	*28*	*97.3*	*2.7*	*380*	*Turned over once by approx. 180°*
S5	*Pellet*	*1.90*	*2*	*16*	*95.1*	*4.9*	*371*	*Turned over once by approx. 180°*
S6	*Pellet*	*1.92*	*2.4*	*17*	*99.0*	*1.0*	*351*	*Turned over thrice by approx. 90°*
S7	*Pellet*	*1.94*	*2.4*	*12*	*95.1*	*4.9*	*323*	*Turned over thrice by approx. 90°*
S8	*Disk*	*1.24*	*2*	*2*	*73.5*	*23.5*	-	*Radius: 7.70 mm*
S9	*Disk*	*0.71*	*2*	*2*	*96.0*	*3.9*	-	*Radius: 5.90 mm*
S10	*Disk*	*0.45*	*2*	*2*	*92.7*	*6.3*	-	*Radius: 4.50 mm*

III.2.1. Pellet reduction

Sample S3 is considered as the reference sample: a non-turned pellet exposed to the light flux during 28 min under 3.5 bars of hydrogen. The temperature profile measured by the thermocouple under the crucible shows a maximum of 371 °C at the end of the experiment (see S.I. Figure E-2). The XRD diffractogram of the reference sample after reduction is provided in S.I. Figure D-3. The reduction yield deduced from the refinement of the curve is 84%, which is too low for an industrial application. In order to improve the efficiency of the

process, the pellet was turned upside down after 14 min of reduction (sample S4), increasing the yield up to 97%.

Then, the possibility i) to reduce the exposure time and ii) to lower the hydrogen pressure was tested to see if it could still lead to an acceptable yield. Provided that no re-oxidation was observed at 2 bars for a pellet of around 2.83 g (see Figure 2), the pressure value was kept at 2 bars or 2.4 bars depending of the pellet mass. As shown in Figure 3, a 7 min reduction is expected to be sufficient to reduce half the pellet. Sample S5 was therefore reduced during two sets of 8 min and was rolled over in between, leading to a reduction yield of 95.1%. Here, a difference between the highest temperature before (357 °C) and after (371 °C) the rolling over is observed. This small difference is probably due to the higher thermal conductivity of metallic iron compared to magnetite.

Finally, it was tested to rotate the pellet 3 times by approx. 90° and to expose it 4 min only between rotations. Samples S6 and S7 show reduction yields of 99.0 % and 95.8% for a total exposure time of 17 min and 12 min, respectively. The XRD diffractogram of sample S6 is available in Figure S.I. D-4. This evidences that rotating pellets under the concentrated light flux remarkedly increases reduction yield and/or decreases reduction time. With regards to temperatures, as for sample S5, a difference in the reached temperature was observed between each phase of the experiment. For S6 the maxima were 313 °C, 329 °C, 351 °C and 348 °C; for S7 they were 302 °C, 315 °C, 323 °C and 322 °C. Here again, the general trend observed is attributed to the higher conductivity of metallic iron. For both samples, the temperature reached during the last part of the reduction is close to the temperature reached during the previous one. This could mean that the reduction is mostly complete after the third phase of the experiment.

One should note that the temperatures measured under the crucible are relatively low compared to the one allowing a fast and complete reduction [32]. However, it is important to keep in mind that the top of the pellet is directly illuminated so it reaches much higher temperatures. As example, during preliminary experiments, a pyrometer was used to measure the surface temperature of powder samples; it was saturated, which indicated temperatures higher than 900 °C. This issue will be fully discussed in section III.3.

XRD analysis of all the samples indicates that, when the reduction is well advanced, the sample is composed of iron and wustite only. This is the case for samples S2, S4, S5, S6, S7, S9 and S10. Nevertheless, for less reduced sample (S1, S3 and S8) the sum of wustite and

iron does not reach 100%, as shown in Table 2. The difference is the amount of magnetite in the sample. For these samples, the temperature was not high enough to fully reduce magnetite into wustite at the end of the experiment.

III.2.2. Gravel reduction

In order to lower the reduction time further, gravels were studied. A single layer of gravel was placed at the bottom of the crucible in order to ensure a complete exposition of the samples. The temperature profile during the experiment on non-turned gravels is available in S.I. Figure E-2. It can be observed that the highest temperature measured under the crucible was 412 °C. XRD analysis evidences that the reduction yield was 88.4% after 28 min, the remaining oxide being wustite only (see Table 2). The second experiment was conducted with the same total exposure time but the gravels were shaken to turn them over after 14 min. A reduction yield of 95% was obtained, which fulfils industrial requirements but remains slightly lower than the one obtained on pellets. The relationship between the reduction yield and the measured temperature under the crucible will be discussed in section III.3.

III.2.3. Disk reduction

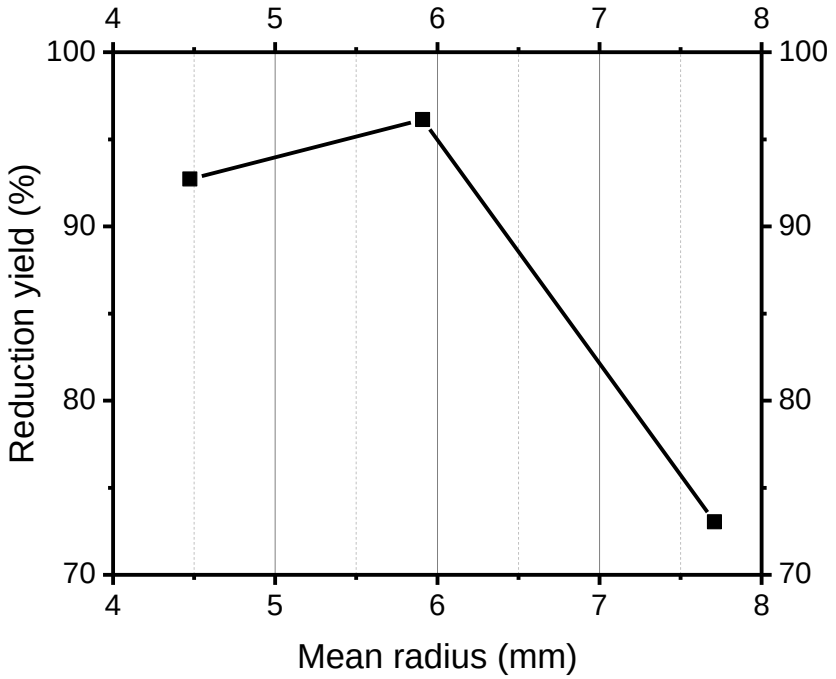

Figure 6: Reduction yield of disks cut into industrial iron ore pellets as a function of their mean radius. The lamp flux density was 60 W/cm², hydrogen pressure 2 bars and reduction time 2 min.

Experiments conducted on pellets have shown that the reduction front has moved of ca. 2 mm after 2 min of exposure (see Figure 4). In order to optimize the process, disks with a thickness of 2 mm were cut and studied. The XRD diffractograms of samples S8, S9 and S10 after reduction are available in S.I. Figures E-4, E-5 and E-6, respectively. They show the presence of wustite and magnetite for S8 and S10, with more intense peaks in the case of S8. Figure 6 shows the reduction yield of the disks after 2 min of exposure under 2 bars of hydrogen.

Large reduction yields of 92% and 96% were obtained for the disks with a radius of 4.75 mm and 5.90 mm, respectively, matching industrial requirements. However, a significant decrease down to 73% occurs for the sample with a radius of 7.70 mm. This decrease was assumed to be related to the non-homogeneity of the light flux in the disk plane. The area where the light flux is more intense is approximately 6 mm in diameter (see Figure 1-c) and can be identified as the whitest spot on the disk in S.I. Table E-1.

Overall, results from section III.2 show that the shape of the iron oxide materials significantly affects reduction time. It is possible to reach low reduction times and large reduction yields when the thickness is reduced. Here, the exposure time was divided by a factor of 14 when going from a 3D sample (single pellet exposed during 28 min) to a 2D one (disk exposed during 2 min). With respect to production rate, it increased by a factor 6 (0.06 g/min to 0.36 g/min) when going from pellet to disk. This shows that the sample size and shape is a really important parameter in the performance of the process.

III.2.4. Energetical efficiency

For the sake of comparison with future developments and other processes, the energy efficiency of the experiments was estimated. Efficiencies were calculated for the most representative cases: the pellet not turned over (S3), one of the pellets turned over (S7) and one of the disks (S9). The efficiency is defined as the theoretical energy required to heat and reduce the sample (E_{th}) divided by the measured energy of the incoming light on the area of the crucible (E_l), as explained in section II. Details on the calculations are provided in S.I. section G. Results are displayed in Table 3 for three temperatures ranging from 500 °C to 1500 °C. The lower bound of this range corresponds to the lowest temperature allowing a complete reduction [33]. The upper bound is the fusion temperature of iron, which was never observed in any of our experiments. As expected for experiments performed on single objects in a non-thermally optimized reactor, the absolute efficiency values are quite low due to thermal losses by radiation and convection. However, the efficiency values increase by a

factor 6 (respectively 2.47) between S3 and S9 (respectively S7), evidencing quantitatively the interest in turning the pellets or using flat samples.

Table 3 : Energy to heat and reduce the sample (E_{th}), energy output of the simulator for each sample (E_l) and energy efficiency as the ratio between the two values.

Sample	E_{th} (J)			E_l (J)	Efficiency (%)		
	500 °C	1000 °C	1500 °C		500 °C	1000 °C	1500 °C
S3	971	1505	2039	201600	0.48	0.75	1.01
S7	1142	1751	2360	86400	1.32	2.03	2.73
S9	424	647	870	14400	2.95	4.49	6.04

III.3. Discussion

In the present section, three worthwhile points will be discussed: i) the temperature of the samples and its link with the reduction mechanism, ii) the scaling-up and potential industrialisation of such a process, and iii) the potential environmental interest of such process.

In the process studied here, the pictures of the cut pellets (see Figure 3-a and 3-b and S.I. Figures C-2, C-3, D-1 and D-2) show that the top of the pellet react first. One could think to two hypotheses to explain it, related to two different limiting factors: i) the temperature is larger at the top ii) the hydrogen does not reach easily the bottom of the pellet because it is sunk into the crucible. The second hypothesis has been excluded by performing an experiment where a pellet was hold onto the top of a small tripod, without any potential limit to hydrogen access. No change in the asymmetry of the reduction was observed, indicating that the limiting factor of the reduction process is temperature and not hydrogen diffusion around the pellet. The mechanism of diffusion of the hydrogen into the pellets is well known. It consists of a mass transfer of the gaseous hydrogen from the atmosphere to the surface of the pellet, followed by a diffusion of the gas through the macro- and micropores of the pellet to reach the active sites and reduce the oxide. The water vapor exits in the opposite way [32], [34]. Additionally, when iron is formed around the sample, is it possible for hydrogen to diffuse through it [32], [34].

The clear frontier between the iron oxide phase and the iron(0) observable on all the pictures of cut pellets suggests the presence of an isotherm. The heat being provided by a direct illumination of the samples, having access to the temperature of this isotherm is not an easy

task as the temperature is expected to be strongly inhomogeneous. In experiments (not shown) where the top surface temperature of the sample has been measured using a pyrometer, values above the upper limit of our apparatus (900 °C) were obtained. Since the iron formed at the top of the pellet has not melt during any of the experiments, the temperature necessarily stays below 1500 °C (iron fusion temperature). On the other hand, the temperature measured just below the crucible (see Figure 1-a) after 28 min was 371 °C for the pellet (see S.I. Figure E-2). Thus, the temperature of the sample during the reaction lies between 1500 °C and this last value (371 °C). A rough estimate of the isotherm value is provided by combining the reduction front speed deduced from Figure 4 (2 mm/min at the beginning and 0.3 mm/min before reaction plateaus) and the experiments by Turkdogan et Vinters on the link between reaction temperature and size of pellets [35]. Using their data, it is estimated that the isotherm value varies from above 1000 °C at the beginning of the reaction to roughly 800 °C when the front speed equals 0.3 mm/min.

For the reduction of gravel, it might, at first sight, seems counter-intuitive that the temperature measured under the crucible was higher for the gravel than for the pellet (412 °C vs 371 °C; cf S.I. Figure E-2) whereas the reduction yield was smaller. This observation could be explained by several phenomena: i) a smaller temperature gradient due to the smaller size of the gravel, ii) an increase of thermal losses due to their larger surface-to-volume ratio, iii) an incomplete coverage of the crucible by the gravel so that parts of its bottom are directly exposed to the light flux, iv) a slow-down of the reduction rate for small samples as observed previously by Turkdogan et Vinters [35] and v) the heat stored by the gravel because of the smaller mass of the sample. Presently available experimental data are not sufficient to decide between these various hypotheses.

In term of scale-up, high concentration ratio technologies like dish or central receivers produce large enough temperature (> 800 °C) to allow hydrogen-based reduction. Given the results provided in the present article, it seems that two different types of reactors could be considered when working with a direct concentrated solar flux. Firstly, moving reactors like rotary kiln or rotating cylindrical reactor have already been studied for high temperature concentrated solar based thermochemical process [36], [37], [38]. This kind of reactor could allow for an advantageous random but continuous rotation of the pellets since it has been shown here that the slowing down of the reaction can be overcome when rotating the pellets. Secondly, in the view of the results with the disk samples, a new reactor in which a few millimetre-thick plates or chips of iron oxide would slide through the light flux on a conveyer

belt type reactor could potentially be interesting. These paths will be explored in future experiments.

Solar facilities only count on renewable energy during their use phase, which is a clear advantage compared to the fossil-fuel based equivalent processes. However, such solar facilities are generally much more material-intensive and therefore energy-intensive during their building phase than standard processes due to the necessity to produce and hold in place large areas of reflectors. The potential savings of CO_2 emissions and reduction of other environmental impacts of solar metallurgy should be studied using life cycle assessment. This will be the subject of future studies. As a preliminary study, our group has recently shown that cooking with parabolic solar cookers compared to standard devices strongly reduce impacts [39]. It is possible to provide a very rough range for the CO_2 emissions of a potential hydrogen-based solar process. As recalled in the introduction, a non-solar hydrogen-based electrically-produced steel consumes 3.5 MWh/t, among which 70% comes from the hydrogen production, the remaining being the energy to heat the ore and melt the DRI [14]. With a low-carbon electricity mix such as the French one (86 gCO_{2eq}/kWh [40]), the non-solar process would emit 301 $kgCO_{2eq}$/t of steel. With a carbon intensive electricity mix such as the Australian one (943 gCO_{2eq}/kWh [41]), the impact is more than ten times higher (3300 $kgCO_{2eq}$/t). These numbers have to be compared with the 522 $kgCO_{2eq}$/t and 1048 $kgCO_{2eq}$/t for the natural gas-based DRI and the coal-based, respectively. Concentrated solar power could replace the energy required to heat the ore and melt the DRI. The lower limit for the emissions is calculated by assuming that the solar concentrator would have zero emissions on its entire life cycle. This would drop the global emissions by 30%, reaching 210 $kgCO_{2eq}$/t and 2300 $kgCO_{2eq}$/t of steel for the French and the Australian electricity mix, respectively. These basic calculations show that combining concentrated solar power and green hydrogen production could drop the CO_2 emissions by at most a factor 5 compared to coal-based DRI. It also illustrates that using hydrogen with an electricity mix intensive in CO_2 is, on the contrary, of no interest.

IV. Conclusion

An alternative ironmaking process based on a concentrated light flux and hydrogen was studied using industrial iron ore pellets. It was first demonstrated that the hydrogen pressure does not have a strong impact on the dynamics of the process as long as the partial water vapor is kept well below the one of hydrogen. It is also shown that using direct light as the

heating source induces a reduction mechanism different from the shrinking core model describing standard processes: here, reduction starts from the illuminated surface towards the shadowed side, due to the large temperature gradient inside the sample. This naturally conducted us to perform experiments in which the pellets were rotated, consequently reducing exposure time. On single pellets, a reduction yield of 96% was reached in 12 min by turning them three times during the exposure. Other shapes of samples seem more suitable to a reduction under light flux than spherical pellets so gravels and flat disks were tested. If the former did not lead to significant improvement, results obtained on the latter were quite impressive: a 2 mm thick disk reached a 96% reduction yield after only 2 min of exposure.

Our results show that, for an efficient process, two parameters need particular attention : i) the thickness of the sample (few millimetres depending on the power) and ii) the atmosphere pressure (H_2:Fe ratio needs to be at least 2.35:1) to avoid the re-oxydation. Additionally, it is also shown that energy efficiency increases with both pressure and power. With these considerations, for an optimized reactor, flat foils or chips of iron ore placed under the solar flux might be a path to envisage. Optimizing such a process requires further simulations of the gas diffusion as well as the temperature distribution into the sample. These points are currently being studied by collaborators [42]. Once the reactor set and the process optimized, it will be mandatory to perform life cycle assessments following several scenarios to study the potential ecological advantage of this process.

The scale at which such a process could be advantageously envisaged is hard to determine. In our view, such a solar process could only make sense in a society that seriously considers sufficiency as a way to preserve human life as we know it as long as possible on our planet. The "right" scale for this process should therefore be determined by considering the geographical distribution of the production units and the global production level.

Acknowledgements

The authors thanks Marion Luu for her help in some experiments, Simon Cayez for XRD and MAUD training, Touati Douar for mechanical and technical support, Catherine Crouzet for electronics engineering and Stéphane Abanadès et Sylvain Rodat (PROMES lab, Odeillo, France) for fruitful discussions. The authors also thanks ArcelorMittal for the raw material supply. This study has been supported by the Agence Nationale de la Recherche (contract ANR-20-CE05-0008-03, METASOL) and INSA Toulouse for the funding of B. Sanglard's PhD.

References:

[1] World Steel association, ‘Steel’s contribution to a low carbon future and climate resilient societies’, 2017, [Online]. Available: https://www.steel.org.au/getattachment/48e75f3b-e33c-43e3-b3e8-b07b330293ae/Position_paper_climate_2017.pdf

[2] L. Holappa, ‘A General Vision for Reduction of Energy Consumption and CO2 Emissions from the Steel Industry’, *Metals*, vol. 10, no. 9, p. 1117, Aug. 2020, doi: 10.3390/met10091117.

[3] Z. Fan and S. J. Friedmann, ‘Low-carbon production of iron and steel: Technology options, economic assessment, and policy’, *Joule*, vol. 5, no. 4, pp. 829–862, Apr. 2021, doi: 10.1016/j.joule.2021.02.018.

[4] J. Astier, ‘Réduction directe’, *Techniques de l’ingénieur Métaux ferreux : élaboration du métal primaire*, vol. base documentaire : TIB366DUO., no. ref. article : m7580. Editions T.I., 2005. [Online]. Available: https://www.techniques-ingenieur.fr/base-documentaire/materiaux-th11/metaux-ferreux-elaboration-du-metal-primaire-42366210/reduction-directe-m7580/

[5] T. Ariyama and M. Sato, ‘Optimization of Ironmaking Process for Reducing CO2 Emissions in the Integrated Steel Works’, *ISIJ Int.*, vol. 46, no. 12, pp. 1736–1744, 2006, doi: 10.2355/isijinternational.46.1736.

[6] H. Suopajärvi, E. Pongrácz, and T. Fabritius, ‘Bioreducer use in Finnish blast furnace ironmaking – Analysis of CO2 emission reduction potential and mitigation cost’, *Appl. Energy*, vol. 124, pp. 82–93, Jul. 2014, doi: 10.1016/j.apenergy.2014.03.008.

[7] F. Patisson and O. Mirgaux, ‘Hydrogen Ironmaking: How It Works’, *Metals*, vol. 10, no. 7, p. 922, Jul. 2020, doi: 10.3390/met10070922.

[8] A. Heidari, N. Niknahad, M. Iljana, and T. Fabritius, ‘A Review on the Kinetics of Iron Ore Reduction by Hydrogen’, p. 19, 2021.

[9] D. Wagner, O. Devisme, F. Patisson, and D. Ablitzer, ‘A laboratory study of the reduction or iron oxides by hydrogen’, Aug. 2006.

[10] M. E. Choi and H. Y. Sohn, ‘Development of green suspension ironmaking technology based on hydrogen reduction of iron oxide concentrate: rate measurements’, *Ironmak. Steelmak.*, vol. 37, no. 2, pp. 81–88, Feb. 2010, doi: 10.1179/030192309X12506804200663.

[11] ‘MIDREX Process’, Midrex Technologies, Inc. Accessed: Apr. 07, 2023. [Online]. Available: https://www.midrex.com/technology/midrex-process/

[12] ‘Hybrit’, Hybrit. Accessed: Apr. 07, 2023. [Online]. Available: https://www.hybritdevelopment.se/en/

[13] S. Hosokai, Y. Kasiwaya, K. Matsui, N. Okinaka, and T. Akiyama, ‘Ironmaking with Ammonia at Low Temperature’, *Environ. Sci. Technol.*, vol. 45, no. 2, pp. 821–826, Jan. 2011, doi: 10.1021/es102910q.

[14] V. Vogl, M. Åhman, and L. J. Nilsson, ‘Assessment of hydrogen direct reduction for fossil-free steelmaking’, *J. Clean. Prod.*, vol. 203, pp. 736–745, Dec. 2018, doi: 10.1016/j.jclepro.2018.08.279.

[15] World Steel association, ‘World steel in figures’, 2024.

[16] Ember, ‘Global electricity review 2024’, May 2024.

[17] M. Pathak, R. Slade, P. R. Shukla, J. Skea, R. Pichs-Madruga, and D. Ürge-Vorsatz, ‘Technical Summary. In: Climate Change 2022: Mitigation of Climate Change. Contribution of Working Group III to the Sixth Assessment Report of the Intergovernmental Panel on Climate Change’. [Online]. Available: doi: 10.1017/9781009157926.002.

[18] A. Steinfeld and E. A. Fletcher, ‘Theoretical and experimental investigation of the carbonthermix reduction of Fe2O3 using solar energy’, *Energy*, vol. 16, no. 7, pp. 1011–1019, Aug. 1991, doi: https://doi.org/10.1016/0360-5442(91)90061-P.
[19] A. Steinfeld, P. Kuhn, and J. Karni, ‘High-temperature solar thermochemistry : Production of iron and synthesis gas by Fe3O4-reduction with methane’, *Energy*, vol. 18, no. 3, pp. 239–249, 1993, doi: 10.1016/0360-5442(93)90108-P.
[20] D. Fernández-González, J. Prazuch, Í. Ruiz-Bustinza, C. González-Gasca, J. Piñuela-Noval, and L. Verdeja González, ‘Iron Metallurgy via Concentrated Solar Energy’, *Metals*, vol. 8, no. 11, p. 873, Oct. 2018, doi: 10.3390/met8110873.
[21] S. Li, H. Zhang, J. Nie, R. Dewil, J. Baeyens, and Y. Deng, ‘The Direct Reduction of Iron Ore with Hydrogen’, *Sustainability*, vol. 13, no. 16, p. 8866, Aug. 2021, doi: 10.3390/su13168866.
[22] S. Abanades and S. Rodat, ‘Solar-aided direct reduction of iron ore with hydrogen targeting carbon-free steel metallurgy’, *Renew. Energy*, vol. 235, no. 121297, 2024, doi: https://doi.org/10.1016/j.renene.2024.121297.
[23] L. Brinkman, B. Bulfin, and A. Steinfeld, ‘Thermochemical Hydrogen Storage via the Reversible Reduction and Oxidation of Metal Oxides’, *Energy Fuels*, vol. 35, no. 22, pp. 18756–18767, Nov. 2021, doi: 10.1021/acs.energyfuels.1c02615.
[24] L. Lu, J. Pan, and D. Zhu, ‘Quality requirements of iron ore for iron production’, in *Iron Ore*, Elsevier, 2015, pp. 475–504. doi: 10.1016/B978-1-78242-156-6.00016-2.
[25] A. Ghosh and A. Chatterjee, *Ironmaking and steelmaking: theory and practice*, 3. print. in Eastern economy edition. New Delhi: PHI Learning, 2010.
[26] J. Pang, P. Guo, and P. Zhao, ‘Reduction kinetics of fine iron ore powder in mixtures of H2-N2 and H2-H2O-N2 of fluidized bed’, *J. Iron Steel Res. Int.*, vol. 22, no. 5, pp. 391–395, May 2015, doi: 10.1016/S1006-706X(15)30017-0.
[27] L. von Bogdandy and H.-J. Engell, *The Reduction of Iron Ores*. Berlin, Heidelberg: Springer Berlin Heidelberg, 1971. doi: 10.1007/978-3-662-10400-2.
[28] O. Levenspiel, *Chemical reaction engineering. Hauptbd.*, 3. ed. New York Weinheim: Wiley, 1999.
[29] A. Bonalde, A. Henriquez, and M. Manrique, ‘Kinetic Analysis of the Iron Oxide Reduction Using Hydrogen-Carbon Monoxide Mixtures as Reducing Agent’, *ISIJ Int.*, vol. 45, no. 9, pp. 1255–1260, 2005, doi: 10.2355/isijinternational.45.1255.
[30] D. Wagner, ‘Etude expérimentale et modélisation de la réduction du minerai de fer par l’hydrogène’, Ph.D Thesis, Institut National Polytechnique de Lorraine, Nancy, 2008. [Online]. Available: https://hal.univ-lorraine.fr/tel-01753016/document
[31] A. Ranzani Da Costa, ‘La réduction du minerai de fer par l’hydrogène : étude cinétique, phénomène de collage et modélisation’, Ph.DThesis, Insitut National Polytechnique de Laurraine, Nancy, 2011. [Online]. Available: https://theses.hal.science/tel-01204934/file/These_Ranzani_2011.pdf
[32] D. Spreitzer and J. Schenk, ‘Reduction of Iron Oxides with Hydrogen—A Review’, *Steel Res. Int.*, vol. 90, no. 10, p. 1900108, Oct. 2019, doi: 10.1002/srin.201900108.
[33] H. Lin, Y.-W. Chen, and C. Li, ‘The mechanism of reduction of iron oxide by hydrogen’, *Thermochim. Acta*, vol. 400, no. 1–2, pp. 61–67, Apr. 2003, doi: https://doi.org/10.1016/S0040-6031(02)00478-1.
[34] C. Feilmayr, A. Thurnhofer, F. Winter, H. Mali, and J. Schenk, ‘Reduction Behavior of Hematite to Magnetite under Fluidized Bed Conditions’, *ISIJ Int.*, vol. 44, no. 7, pp. 1125–1133, 2004, doi: 10.2355/isijinternational.44.1125.
[35] E. T. Turkdogan and J. V. Vinters, ‘Gaseous reduction of iron oxides: Part I. Reduction of hematite in hydrogen’, *Metall. Mater. Trans. B*, vol. 2, no. 11, pp. 3175–3188, Nov. 1971, doi: 10.1007/BF02814970.

[36] G. Flamant, D. Gauthier, C. Boudhari, and Y. Flitris, ‘A 50 kW Fluidized Bed High Temperature Solar Receiver: Heat Transfer Analysis’, *J. Sol. Energy Eng.*, vol. 110, no. 4, pp. 313–320, Nov. 1988, doi: 10.1115/1.3268273.
[37] S. Abanades, P. Charvin, and G. Flamant, ‘Design and simulation of a solar chemical reactor for the thermal reduction of metal oxides: Case study of zinc oxide dissociation’, *Chem. Eng. Sci.*, vol. 62, no. 22, pp. 6323–6333, Nov. 2007, doi: 10.1016/j.ces.2007.07.042.
[38] M. Neises, S. Tescari, L. de Oliveira, M. Roeb, C. Sattler, and B. Wong, ‘Solar-heated rotary kiln for thermochemical energy storage’, *Sol. Energy*, vol. 86, no. 10, pp. 3040–3048, Oct. 2012, doi: 10.1016/j.solener.2012.07.012.
[39] B. Sanglard, S. Lachaize, J. Carrey, and L. Tiruta-Barna, ‘Life cycle assessment of a parabolic solar cooker and comparison with conventional cooking appliances’, *Sustain. Prod. Consum.*, vol. 42, pp. 211–233, Nov. 2023, doi: 10.1016/j.spc.2023.09.018.
[40] IEA World Energy Statistics and Balances, ‘Ecoinvent 3.8 Dataset Documentation “market for electricity, low voltage - FR - electricity, low voltage”’. OECD.
[41] IEA World Energy Statistics and Balances, ‘Ecoinvent 3.8 Dataset Documentation “market for electricity, low voltage - AU - electricity, low voltage”’. OECD.
[42] A. Skaf, L. Tiruta-Barna, and A. Ahmadi, ‘Assessing the potential of low-temperature ironmaking using pure hydrogen in shaft reactors’, *Submitted to Chemical engineering and processing- Process intensification*, 2024.